VOL. 13, NO. 23, DECEMBER 2018 ISSN 1819-6608
ARPN Journal of Engineering and Applied Sciences

www.arpnjournals.com

ADAPTIVE NONLINEAR MPPT CONTROL FOR PV SYSTEM WITH RESONANT DC/DC CONVERTER

M. Et-Taoussi[1], H. Ouadi[1], F. Giri[2] and S. Diouny[3]
[1]PMMAT Lab, Department of Physics, Faculty of Science, Aîn-Chock, Hassan II University, Casablanca, Morocco
[2]GREYC Lab, Automatic Department, Caen University, Caen, France
[3]Linguistics Lab, Department of English, Chouaib Doukkali University, El-Jadida, Morocco
E-Mail: mehdiettaoussi@rocketmail.com

ABSTRACT

In this paper, the Maximum Power Point Tracking (MPPT) problem for photovoltaic (PV) system is investigated. The considered PV system includes a PV Generator (PVG) connected to DC bus using a DC/DC Converter. Unlike standard PV systems, the used static converter is of the series resonant type (SRC). Indeed, this latter optimizes the power losses during the switching phases. Furthermore, to provide easy maintenance and increase reliability and cost effectiveness of photovoltaic systems, the developed MPPT control is implemented without needing any solar sensor. The proposed nonlinear controller (NLC) is of adaptive type in order to provide a reliable online-estimate of uncertain parameters namely those depending on solar irradiance. Indeed, two main difficulties arise when designing this adaptive controller (NLC): *(i)* several nonlinearities and discontinuities appear in the resonant converter model; *(ii)* The convergence of the estimated parameters to their real values is required for achieving the MPPT objective. A formal analysis exhibits that the designed controller is able to extract the PVG optimal power. Numerical simulations are performed to highlight the tracking performances.

Keywords: PV generator, series resonant DC/DC converter, MPPT, sensorless solar irradiance controller, nonlinear adaptive controller, backstepping control design.

1. INTRODUCTION

Thermal power plants (e.g. oil, diesel oil, coal or gas) produce two thirds of the world's electricity [1]. However, they emit pollutants, responsible for climate deterioration and depletion of natural resources. Thus, the deployment of renewable energy remains an alternative to the phasing out of fossil fuels. In this context, photovoltaic industry has gained widespread popularity in the past decade, for its efficiency and low cost of manufacturing solar panels. In general, the photovoltaic generator (PVG) consists of several solar panels which are connected to the DC-bus through a DC-DC converter (see Figure-1).

Recall that the generated electric power is influenced by climatic conditions, namely temperature and solar irradiance [2]. Figure-2 shows the general shape of the Power/Voltage PVG characteristic. Indeed, when the PVG is exposed to variable solar irradiance levels, its operating voltage must be controlled so that the corresponding Power/Voltage point is kept around the Maximum Power Point (MPP) [3, 4, 5]. This tracking objective is generally called "MPPT" (Maximum Power Point Tracking) [6].

There exist several studies where the MPPT objective for PV system has been addressed (e.g. [6, 7]). Most of these previous works assume that the solar irradiance measure is available. However, the solar irradiance sensors suffer from a lack of precision and efficiency caused by environmental factors. Moreover, the installation and maintenance of these sensors cost generally expensive. Thus, it is recommended to develop a MPPT controller without resorting to the solar irradiance measurement.

Furthermore, with regard to the used MPPT control technique, we can classify previous work into three categories. The first class of controllers uses artificial intelligence approaches (fuzzy logic controller and artificial neural networks) [8, 9]. For this category, the PV system accurate model is not used when designing the controller. Therefore, there is no formal analysis to evaluate the obtained control performances. The second class includes linear MPPT controllers [10]. The latter are designed using a linear approximation of the PV system model. In fact, the PV system nonlinearities are neglected in the control design and consequently, the controller performances are limited especially when the solar irradiance varies within a wide range. In the third category, nonlinear MPPT regulators are performed using various design techniques. For instance, in [11, 12] the MPPT objective is achieved using Backstepping and Sliding-mode controller, respectively. Nevertheless, both proposed controllers require solar irradiance measurement.

The sensorless MPPT controller design, involving the nonlinear model of PV system was addressed in [13]. The considered PV system is equipped with a boost converter. The sensorless solar irradiance control was performed by combining a Backstepping controller with a solar irradiance adaptive algorithm. However, the use of a forced switching converter (with relatively high switching frequency) results in a negative impact on the photovoltaic system efficiency. Indeed, it is well known that for the forced switching converter, the losses increase, on the one hand, with the switching of frequency, and on the other hand, with the magnitude of current to be switched. It is therefore advantageous to use natural switching converter. Indeed, resonant DC/DC offers a relatively high efficiency compared to forced switching converter (see Section 4.4).

In this paper, an efficient and relatively low-cost solution for the PVG MPPT control is developed. Indeed,

the optimality of the proposed MPPT control lies on the one hand in the use of a resonant converter providing better efficiency (compared to the conventional boost converter) and on the other hand to the removal of the solar irradiance sensor. Following the generalized averaging method [14], the considered PV system (consisting of PVG, DC/DC resonant power converter and DC bus, see Figures 1, 4) is represented by a state-space model. This state representation involves five state variables with a single control signal (the converter switching frequency). Regarding the control design, three difficulties arise: *(i)* PV system involves highly nonlinear model; *(ii)* some PV system parameters are unknown; *(iii)* the control input is involved in most of the state equations. Then, using the Backstepping technique, an adaptive MPPT controller is developed without resorting to solar irradiance sensor [15, 16, 17].

The paper is structured as follows: Section 2 is devoted to the system modeling. Section 3 outlines the controller development.

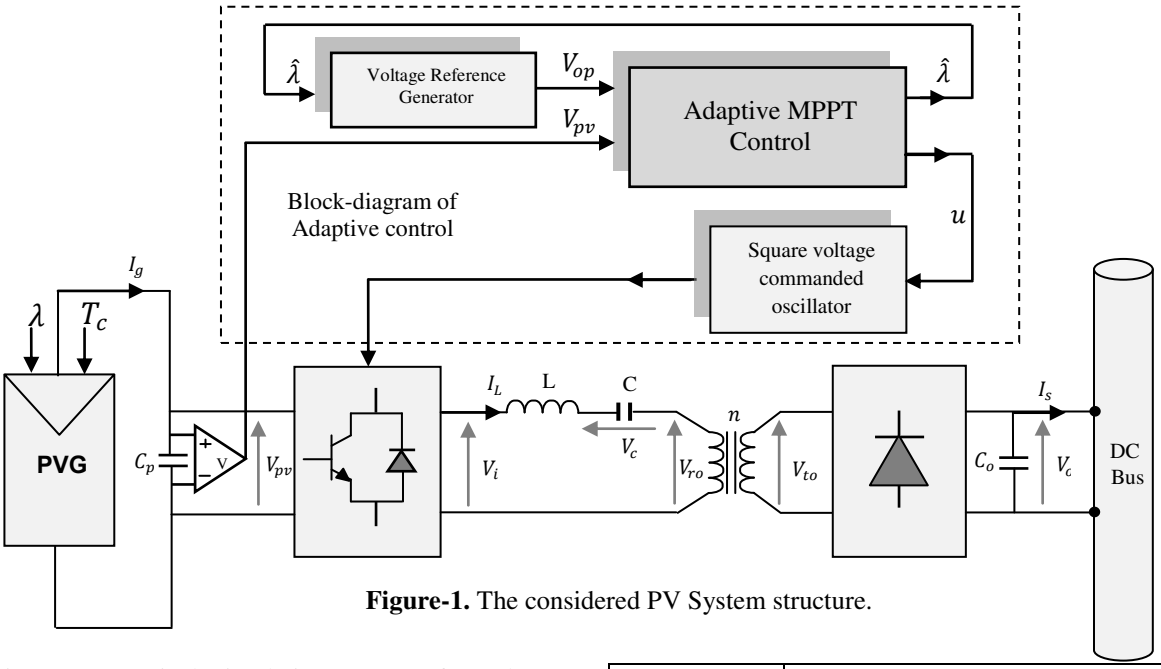

Figure-1. The considered PV System structure.

In Section 4, numerical simulations are performed to compare the performances of the proposed controller with that of the conventional MPPT regulators. The paper ends with a conclusion and bibliographic references.

Table-1. List of notations.

Parameter	Designation
λ	Solar irradiance
I_g	PV Generator current
I_{ph}	Photocurrent of PV cell
I_{rs}	Cell reverse saturation current
T_c	Cell temperature
n_p	parallel PV cells
n_s	series PV cells
I_{scr}	STC short-circuit current
k	Boltzmann's constant
q	Electron charge
A	PV cell ideality factor
K_i	Short circuit temperature coefficient
T_r	Reference temperature
V_{pv}	PVG voltage
V_{op}	Optimal PVG voltage
P_{op}	Optimal PVG power
V_i	Inverter output voltage
V_o	Resonant converter output voltage
V_{ro}	Transformer primary voltage
V_{to}	Rectifier input voltage
I_L	Resonant tank current
I_s	Resonant converter output current
V_c	Resonant tank voltage
C_P	Capacitor of inverter DC bus
L	Resonant inductor
C	Resonant capacitor
C_o	DC bus capacitor
n	HF-transformer ratio
f_s	Inverter varying switching-frequency ($w_s = 2\pi f_s$)
α	Phase shift of the current I_L with respect to V_i voltage

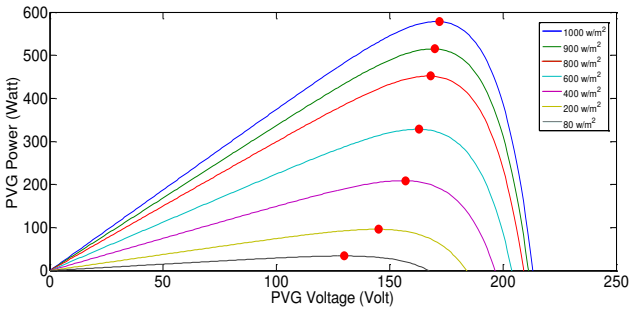

Figure-2. Shape of the Characteristic (V_{pv}, P_{pv}) for different solar irradiances.

2. PHOTOVOLTAIC SYSTEM MODELING

Figure-1 depicts the adopted PV system architecture, which is based on a PV Generator (PVG) and a Series Resonant Chopper (SRC) connected to the DC bus. Recall that the objective is to track the MPP (Maximum Power Point) for PVG.

2.1 Photovoltaic generator model

Various equivalent circuits have been reported in the literature for PV cell modeling. For instance, there is one-diode, two-diode and three-diode model [7, 18]. The equivalent circuit of two-diode and three-diode model can be used to improve the PVG model accuracy [18]. However, due to their strongly nonlinear character, it is very difficult to exploit these model for the control law design [7]. Therefore, the one-diode model is adopted in this study, since it provides sufficient accuracy besides an easier adaptation to the control design. Figure-3 depicts the corresponding electrical circuit [19].

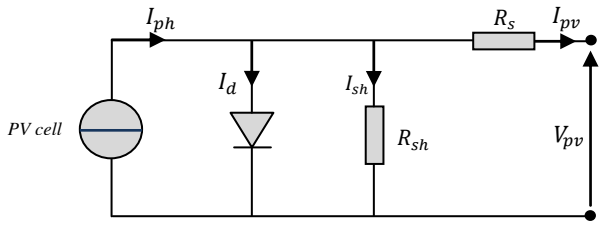

Figure-3. PV Cell equivalent circuit.

With the notation given in Table-1, the one diode ideal model of PVG is governed by the following equation [19, 20]:

$$I_g = I_{phg} - I_{og}\left(exp\left(A_g V_{pv}\right) - 1\right) \quad (1)$$

with $I_{phg} = n_p I_{ph}$, $I_{og} = n_p I_{rs}$

and $$A_g = \frac{q}{n_s A k T_c} \quad (2)$$

where $$I_{ph} = [I_{scr} + K_i(T_c - T_r)] \frac{\lambda}{1000} \quad (3)$$

Note that in this study, the following assumptions are retained for the PVG modeling:

Assumption 1. The solar irradiance value (λ) is considered as uncertain parameter.

Assumption 2. The PVG temperature is assumed to be measurable.

Equation (3) expresses the photocurrent (I_{ph}) as a linear function with respect to the cell solar irradiance (λ). Let's adopt the following notations:

$$I_{phg} = \theta(\lambda) \quad (4)$$

$$\varphi_1(V_{pv}) = exp(A_g V_{pv}) - 1 \quad (5)$$

Then equation (1) becomes:

$$I_g = \theta(\lambda) - I_{og}\varphi_1(V_{pv}) \quad (6)$$

2.2 Resonant converter modeling

The conventional used chopper is the Boost. This later is a non-isolated and a forced switching converter. Consequently the Boost power losses during the switching phases are relatively high. Reducing these losses requires the implementation of an auxiliary network, usually dissipative, complex and expensive [21].

Furthermore, resonant DC/DC converter has attracted more interest for their use in the last decades. In fact, it is an isolated converter, and these switches operate in smooth switching. This allows reducing significantly the converter power losses [21, 22]. Moreover, resonant converter makes a better use of a high frequency range and power. Consequently, the passive components volume is reduced. Figure-4 describes the adopted structure of series resonant converter.

Several studies were interested in the problem of resonant DC/DC modeling (e.g. [22, 23]). Most of these works consider the case where the resonant converter is fed by a voltage source. This is not the case for the system in study since the PVG is represented by a DC current source.

Using the basic laws of electricity according to the converter circuit, one obtains the following physical model [24]:

$$\frac{di_L(t)}{dt} = \frac{v_{pv}(t)}{L} \mathrm{Sgn}(2\pi f_s t) - \frac{v_c(t)}{L} - \frac{v_0(t)}{nL} \mathrm{Sgn}(2\pi f_s t - \alpha) \quad (7)$$

$$\frac{dv_c(t)}{dt} = \frac{1}{C} i_L(t) \quad (8)$$

$$\frac{dv_{pv}(t)}{dt} = \frac{i_g(t)}{C_p} - \frac{1}{C_p} abs(i_L(t)) = \frac{i_g(t)}{C_p} - \frac{1}{C_p} i_L(t)\, \mathrm{Sgn}(2\pi f_s t - \alpha) \quad (9)$$

The above model Equations (7-9) is quite suitable to describe the operation of the system; however, due to its complexity (the model above has a nonlinear structure and involves a binary control input); it seems not adapted to the control design. Hence, an approximate model is developed using the generalized averaging method [14].

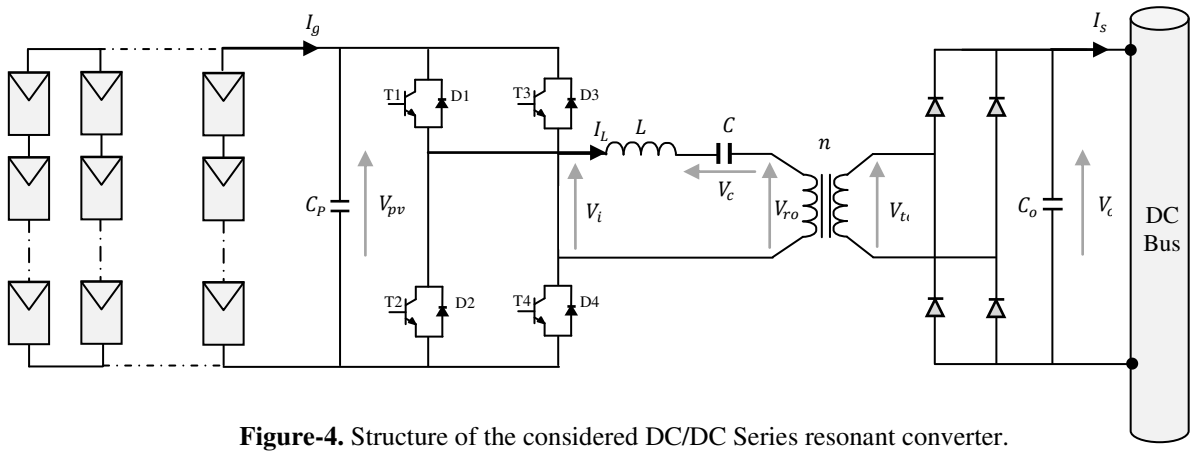

Figure-4. Structure of the considered DC/DC Series resonant converter.

In the following, the corresponding Generalized Average Model (GAM) is developed on the basis of the following assumptions [25]:

Assumption 3. Near the resonance frequency, V_c voltage and current I_L are considered sinusoidal, this makes their first harmonic approximation acceptable (respectively by V_1 and $I_1 e^{-j\alpha}$).

Assumption 4. The capacitors C_p and C_o values are assumed large enough to consider that the voltages (respectively V_{pv} and V_o) at their terminals are slowly variable.

According to [14], the first-harmonic PV system model is given as follows:

$$\frac{dI_1}{dt} = -jw_s I_1 + \frac{1}{L}\left[-V_1 - \frac{2}{jn\pi} V_o\, e^{-j\alpha} + \frac{2V_{pv}}{j\pi}\right] \quad (10)$$

$$\frac{dV_1}{dt} = -jw_s V_1 + \frac{1}{C} I_1 \quad (11)$$

$$\frac{dV_{PV}}{dt} = \frac{I_g}{C_p} - \frac{1}{C_p}\left[\frac{4}{\pi}\|I_1\|\right] \quad (12)$$

The last model Eqs.(10-12) is not adapted to the control design due to these complex parameters. To obtain an appropriate model, let's introduce the following notations:

$$I_1 = x_1 + jx_2\ ,\ V_1 = x_3 + jx_4 \text{ and } V_{pv} = x_5 \quad (13)$$

By replacing the latter Equation (13) and Equations (1, 4, 5) in Equations (10-12), one gets the following state-space model:

$$\dot{x}_1 = u\, x_2 - \frac{x_3}{L} - \frac{1}{nL}\frac{2V_o}{\pi}\frac{x_2}{\sqrt{{x_1}^2 + {x_2}^2}} \quad (14)$$

$$\dot{x}_2 = -u\, x_1 - \frac{2x_5}{\pi L} - \frac{x_4}{L} + \frac{1}{nL}\frac{2V_o}{\pi}\frac{x_1}{\sqrt{{x_1}^2 + {x_2}^2}} \quad (15)$$

$$\dot{x}_3 = u\, x_4 + \frac{x_1}{C} \quad (16)$$

$$\dot{x}_4 = -u\, x_3 + \frac{x_2}{C} \quad (17)$$

$$\dot{x}_5 = \frac{1}{C_p}\theta(\lambda) - \frac{1}{C_p} I_{og}\varphi_1(x_5) - \frac{4}{\pi C_p}\sqrt{{x_1}^2 + {x_2}^2} \quad (18)$$

$\theta(\lambda)$ is the uncertain parameter and $u = w_s$ is the control input (SRC-Inverter switching frequencies).

Based on the PVG control model Equations (14-18), we propose to design a controller ensuring the MPPT objective.

3. CONTROL DESIGN

3.1 Controller objective

The proposed MPPT control has three objectives:

a) Estimating the solar irradiance.
b) Constructing the optimal PV voltage reference from the solar irradiance estimation.
c) Extracting the maximum power from PVG in presence of a wide range variation of solar irradiance.

To meet these objectives, a nonlinear controller of adaptive type will be developed in three steps according to the Backstepping method [15].

3.2 Voltage reference signal

As illustrated by Figure-2, for a given solar irradiance, there is one reference of PVG voltage which corresponds to the maximum extracted photovoltaic power. In this study, a graphical exploration of maximal power points (MPP) is performed. Indeed, for a set of about twenty irradiance values $\lambda_k (k = 1,2,\dots,20)$ the corresponding optimal power points $\left(V_{op} = V^*_{pv\_k}, P^*_{pv\_k}\right)$ are graphically determined. Then, a polynomial interpolation $P(\lambda)$ was constructed to approach, in the sense of least squares, the set of maximum points $\left(V^*_{pv\_k}, P^*_{pv\_k}\right)$.

For the case studied, the resulting polynomial $P(\lambda)$ is defined by Equation (19) and Table-2.

$$P(\lambda) = h_{10}\lambda^{10} + h_9\lambda^9 + \cdots \dots + h_0 \quad (19)$$

Table-2. List of the polynomial coefficients.

h_{10}	$8.3\ x\ 10^{-27}$	h_5	$4.2\ x\ 10^{-10}$
h_9	$-1.2\ x\ 10^{-23}$	h_4	$-2.3\ x\ 10^{-7}$
h_8	$-7.9\ x\ 10^{-20}$	h_3	$7.3\ x\ 10^{-5}$
h_7	$3.1\ x\ 10^{-16}$	h_2	-0.014
h_6	$-4.8\ x\ 10^{-13}$	h_1	1.6
		h_0	64

The shape of the polynomial $P(\lambda)$ is plotted in Figure-5.

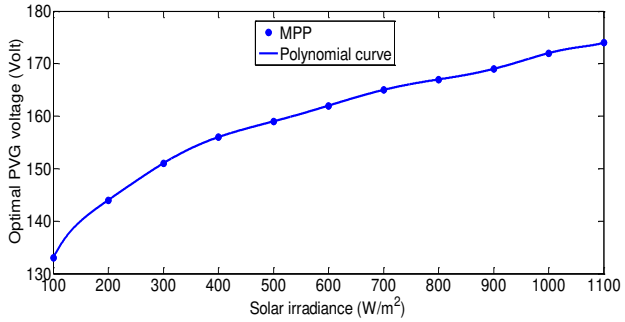

Figure-5. Optimal voltage (V_{op}) (in Volt), according to the solar irradiance λ (in $\mathrm{W/m^2}$).

3.3 Adaptive MPPT controller design

In this section, the controller is designed to achieve the convergence of the PVG voltage (x_5) to its optimal trajectory (reference), denoted x_5^*. The control law will have an adaptation ability to online estimate the unknown parameter (θ). Unlike standard adaptive control problems the convergence of the estimated parameter $(\hat{\theta})$ to its true value (θ) is mandatory for the MPPT objective [15, 16, 17]. Indeed, the θ value is required and expected to compute the solar irradiance for the determination of the PVG voltage reference (see section 3.2).

To design the controller, the next realistic assumption is crucial:

Assumption 5. The reference signal (x_5^*) is assumed to be bounded. Its first, second and third derivatives are also bounded.

Step 1. The design procedure starts by introducing the first tracking error z_1:

$$z_1 = x_5 - x_5^* \tag{20}$$

The objective of the first step is to force the error z_1 to vanish asymptotically. To achieve this, the tracking error is time-derived (using Equations (18, 20)) as follows:

$$\dot{z}_1 = \frac{1}{C_p}\theta(\lambda) - \frac{1}{C_p} I_{og}\varphi_1(x_5) - \frac{4}{\pi C_p}\sqrt{{x_1}^2 + {x_2}^2} - \dot{x}_5^* \tag{21}$$

Let us denote by $\tilde{\theta} = \theta - \hat{\theta}$ the estimated error, and consider the following Lyapunov's candidate function:

$$V_1 = \frac{1}{2}\,{z_1}^2 + \frac{1}{2}\left(\frac{\tilde{\theta}^2}{\gamma}\right) \tag{22}$$

where γ is a real positive parameter related to the control design. This parameter is referred as the '*Adaptation Gain*'.

Deriving V_1 over the trajectory (z_1, θ), gives:

$$\dot{V}_1 = z_1\left(f_1\hat{\theta} - \rho\varphi_1(x_5) - \frac{4}{\pi} f_1\sqrt{{x_1}^2 + {x_2}^2} - \dot{x}_5^*\right) - \tilde{\theta}\left(\frac{\dot{\hat{\theta}}}{\gamma} - z_1 f_1\right) \tag{23}$$

with $\rho = \frac{1}{C_p} I_{og}$

and $f_1 = \frac{1}{C_p}$ (First regressor function) (24)

One could eliminate $\tilde{\theta}$ from Eq.(23) using the following parameter update law:

$$\dot{\hat{\theta}} = \gamma q_1 = \gamma\, z_1 f_1 \tag{25}$$

Furthermore, z_1 could be converging to zero by letting $-\frac{4}{\pi} f_1\sqrt{{x_1}^2 + {x_2}^2} = \beta_1$, where the stabilizing function β_1 is defined by:

$$\beta_1 = -k_1 z_1 - f_1\hat{\theta} + \rho\varphi_1(x_5) + \dot{x}_5^* \tag{26}$$

with k_1 is a real positive parameter for the control design.

Since, the quantity $-\frac{4}{\pi} f_1\sqrt{{x_1}^2 + {x_2}^2}$ does not represent the real control input (virtual control). Then, only the convergence of the error $\left(-\frac{4}{\pi} f_1\sqrt{{x_1}^2 + {x_2}^2} - \beta_1\right)$ to zero can be achieved. Also, $\dot{\hat{\theta}} = \gamma q_1$ does not represent the parameter update law. However, q_1 is considered as the first tuning function while tolerating the $\tilde{\theta}$ presence in $\dot{V}_1$. Accordingly, one defines a second error variable as follows:

$$z_2 = -\frac{4}{\pi} f_1\sqrt{{x_1}^2 + {x_2}^2} - \beta_1 \tag{27}$$

Using Equations (26, 27), $\dot{z}_1$ becomes:

$$\dot{z}_1 = -k_1 z_1 + z_2 + f_1\tilde{\theta} \tag{28}$$

Now, with Equation (28), the Lyapunov function derivative (V_1) becomes:

$$\dot{V}_1 = -k_1 {z_1}^2 + z_1 z_2 - \tilde{\theta}\left(\frac{\dot{\hat{\theta}}}{\gamma} - q_1\right) \tag{29}$$

Step 2. The purpose of this step is to ensure the convergence of $[z_1 \quad z_2]^T$ to $[0 \quad 0]^T$.

To this end, time derivative of z_2 is first determined. Deriving Equation (27), using Equations (14, 15, 26, 28), one obtains:

$$\dot{z}_2 = \frac{8\,f_1(x_2x_5)}{\pi^2 L\sqrt{{x_1}^2+{x_2}^2}} + f_1\dot{\hat{\theta}} + f_2\tilde{\theta} + \psi_1 - \ddot{x}_5^* \quad (30)$$

with $f_2 = k_1 f_1 - \rho A_g f_1 exp(A_g x_5)$ (31)
(Second regressor function)

and

$$\psi_1 = \frac{4\,f_1(x_1x_3+x_2x_4)}{\pi L\sqrt{{x_1}^2+{x_2}^2}} - {k_1}^2 z_1 + k_1 z_2 - \rho A_g exp(A_g x_5)\left(f_1\hat{\theta} - \rho\varphi_1(x_5) - \frac{4\,f_1}{\pi}\sqrt{{x_1}^2+{x_2}^2}\right) \quad (32)$$

Note that the quantity $\frac{8\,f_1x_2x_5}{\pi^2 L\sqrt{{x_1}^2+{x_2}^2}}$ stands in Equation (30) as a virtual control input. Accordingly, a second Lyapunov equation (V_2) is defined as follows:

$$V_2 = V_1 + \frac{1}{2}\,{z_2}^2 \quad (33)$$

Its time derivative is obtained using Equation (29) and Equation (30):

$$\dot{V}_2 = -k_1{z_1}^2 + z_2\left(z_1 + \frac{8\,f_1(x_2x_5)}{\pi^2 L\sqrt{{x_1}^2+{x_2}^2}} + f_1\dot{\hat{\theta}} + \psi_1 - \ddot{x}_5^*\right) - \tilde{\theta}\left(\frac{\dot{\hat{\theta}}}{\gamma} - (q_1 + z_2 f_2)\right) \quad (34)$$

The term $\tilde{\theta}$ can be eliminated in Eq. (34) using the following parameter update law:

$$\dot{\hat{\theta}} = \gamma q_2 = \gamma(q_1 + z_2\, f_2) \quad (35)$$

Let $\left(\frac{8\,f_1(x_2x_5)}{\pi^2 L\sqrt{{x_1}^2+{x_2}^2}} = \beta_2\right)$ denote the second stabilizing function, chosen as:

$$\beta_2 = -z_1 - f_1\dot{\hat{\theta}} - \psi_1 - k_2 z_2 + \ddot{x}_5^* \quad (36)$$

with k_2 is any real positive control design parameter.

Now, with Equation (36) and the above parameter update law (Equation (35)), $\dot{V}_2$ (Equation (34)) would reduce to:

$$\dot{V}_2 = -k_1{z_1}^2 - k_2{z_2}^2 \quad (37)$$

As the quantity $\left(\frac{8f_1x_2x_5}{\pi^2 L\sqrt{{x_1}^2+{x_2}^2}}\right)$ does not correspond to the real control input, the parameter update law Equation (35) is not enough to overcome uncertainty. However, q_2 is considered as the second tuning function. Let's introduce the new error z_3 :

$$z_3 = \frac{8\,f_1x_2x_5}{\pi^2 L\sqrt{{x_1}^2+{x_2}^2}} - \beta_2 \quad (38)$$

Using Equation (36) and Equation (38), Equation (34) becomes:

$$\dot{V}_2 = -k_1{z_1}^2 - k_2{z_2}^2 - z_2 f_1\left(\gamma q_2 - \dot{\hat{\theta}}\right) - \tilde{\theta}\left(\frac{\dot{\hat{\theta}}}{\gamma} - (q_1 + z_2 f_2)\right) + z_2 z_3 \quad (39)$$

Similarly, time derivative of the tracking error z_2 becomes:

$$\dot{z}_2 = -z_1 - k_2 z_2 + z_3 - f_1\left(\gamma q_2 - \dot{\hat{\theta}}\right) + \tilde{\theta} f_2 \quad (40)$$

Using Equation (40) and Equation (28), the error system (z_1, z_2) undergoes the following equation:

$$[\dot{z}_1\ \dot{z}_2]^T = \begin{bmatrix} -k_1 & 1 \\ -1 & -k_2 \end{bmatrix}\begin{bmatrix} z_1 \\ z_2 \end{bmatrix} + \begin{bmatrix} 0 \\ z_3 - f_1\left(\gamma q_2 - \dot{\hat{\theta}}\right) \end{bmatrix} + \begin{bmatrix} f_1 \\ f_2 \end{bmatrix}\tilde{\theta} \quad (41)$$

This will complete **Step 2**.

Remark. The term $(\sqrt{{x_1}^2+{x_2}^2})$ is the first harmonics amplitude of resonant current (I_L), this latter is nonzero as long as the resonant converter operates. ■

Step 3. The aim of this step is to ensure the control errors convergence (z_1, z_2, z_3) towards zero.

Using Equations (14, 15, 18, 36) time derivatives of the tracking error z_3 is obtained in a suitable form as follows:

$$\dot{z}_3 = G.u + f_3\tilde{\theta} - g_2\dot{\hat{\theta}} + \Psi \quad (42)$$

The expressions of the newly introduced parameters (namely: G, f_3, g_2 and Ψ) are given in Appendix B.

At this point, the aim is to seek a control law (u) and an update law $(\hat{\theta})$ that achieve the asymptotic stability of system $(z_1, z_2, z_3, \tilde{\theta})$. For this purpose, let's consider the following Lyapunov function:

$$V_3 = V_2 + \frac{1}{2}\,{z_3}^2 \quad (43)$$

Using Equations (39, 42), time derivative of Eq.(43) becomes:

$$\dot{V}_3 = -k_1{z_1}^2 - k_2{z_2}^2 - z_2 f_1\left(\gamma q_2 - \dot{\hat{\theta}}\right) + \tilde{\theta}\left(-\frac{\dot{\hat{\theta}}}{\gamma} + (q_2 + z_3 f_3)\right) + z_3\left(G\,u - g_2\dot{\hat{\theta}} + \Psi + z_2\right) \quad (44)$$

Equation (44) suggests the choice of the estimated parameter $\hat{\theta}$ as follows:

$$\dot{\hat{\theta}} = \gamma q_3 = \gamma(q_2 + z_3 f_3) \quad (45)$$

where q_3 is the third tuning function.

However, this update law is not convenient due to its integral nature; moreover, the integration of the estimated parameter $\dot{\hat{\theta}}$ could diverge during the closed loop control. This problem can be circumvented by

performing a projection of this estimated parameter on a compact set involving the real parameter [26]. Let's consider a bounded interval D which represents the highest value that can take θ (PVG photocurrent) as $D \geq |\theta|$, and $\hat{\theta}(0)$ is initially chosen so that $\hat{\theta}^2(0) \leq D^2$. We set $D = 4$ Amp, and we define the projection operator $\Lambda(\gamma q_3) = \dot{\hat{\theta}}$ as follows:

$$\Lambda(\gamma q_3) \stackrel{\text{def}}{=} \begin{cases} \gamma q_3 & if \quad \hat{\theta}^2 \leq D^2 \\ 0 & otherwise \end{cases} \tag{46}$$

Furthermore, based on Equation (44), the control law is defined as follows:

$$u = \frac{1}{G}\left(g_2\dot{\hat{\theta}} - \Psi - z_2 - k_3 z_3 + \eta\right) \tag{47}$$

with k_3 is any real positive control design parameter, and η is an supplementary control parameter for dealing with the adaptive law saturation issue. This parameter is set as follows:

$$\eta = \begin{cases} -\gamma f_1 f_3 z_2 & if \quad \dot{\hat{\theta}} = \gamma q_3 \\ 0 & if \quad \dot{\hat{\theta}} = 0 \end{cases} \tag{48}$$

Substituting the adaptive control law Equation (47) in Equation (42), and using Equations (28, 40, 48), we obtain the model of the closed loop control, according to the errors $Z = (z_1, z_2, z_3)$ and $\tilde{\theta}$, as follows:

$$\dot{Z} = \bar{M}Z + F\tilde{\theta} \tag{49}$$

$$\text{with } \dot{Z} = \begin{bmatrix} \dot{z}_1 \\ \dot{z}_2 \\ \dot{z}_3 \end{bmatrix}; \quad Z = \begin{bmatrix} z_1 \\ z_2 \\ z_3 \end{bmatrix};$$
$$\bar{M} = \begin{bmatrix} -k_1 & 1 & 0 \\ -1 & -k_2 & 1+\sigma \\ 0 & -1-\sigma & -k_3 \end{bmatrix}; \; F = \begin{bmatrix} f_1 \\ f_2 \\ f_3 \end{bmatrix} \text{ and } \sigma = \gamma f_1 f_3 \tag{50}$$

The theoretical performance of the control system is described in the next theorem.

Theorem. For the closed-loop control system constituted by the PV system Equations (14-18) and the control law Equations (47, 48) with the parameter update law Equations (45, 46), there is a parameter $k_{min} > 0$, such that, if $inf(k_1, k_2, k_3) > k_{min}$, then:

a) The error vector $[z_1\ z_2\ z_3]^T$ converges asymptotically to $[0\ 0\ 0]^T$.
b) The estimated parameter $\hat{\theta}$ converges to its real value. ■

Proof. The theorem proof is given in Appendix A.

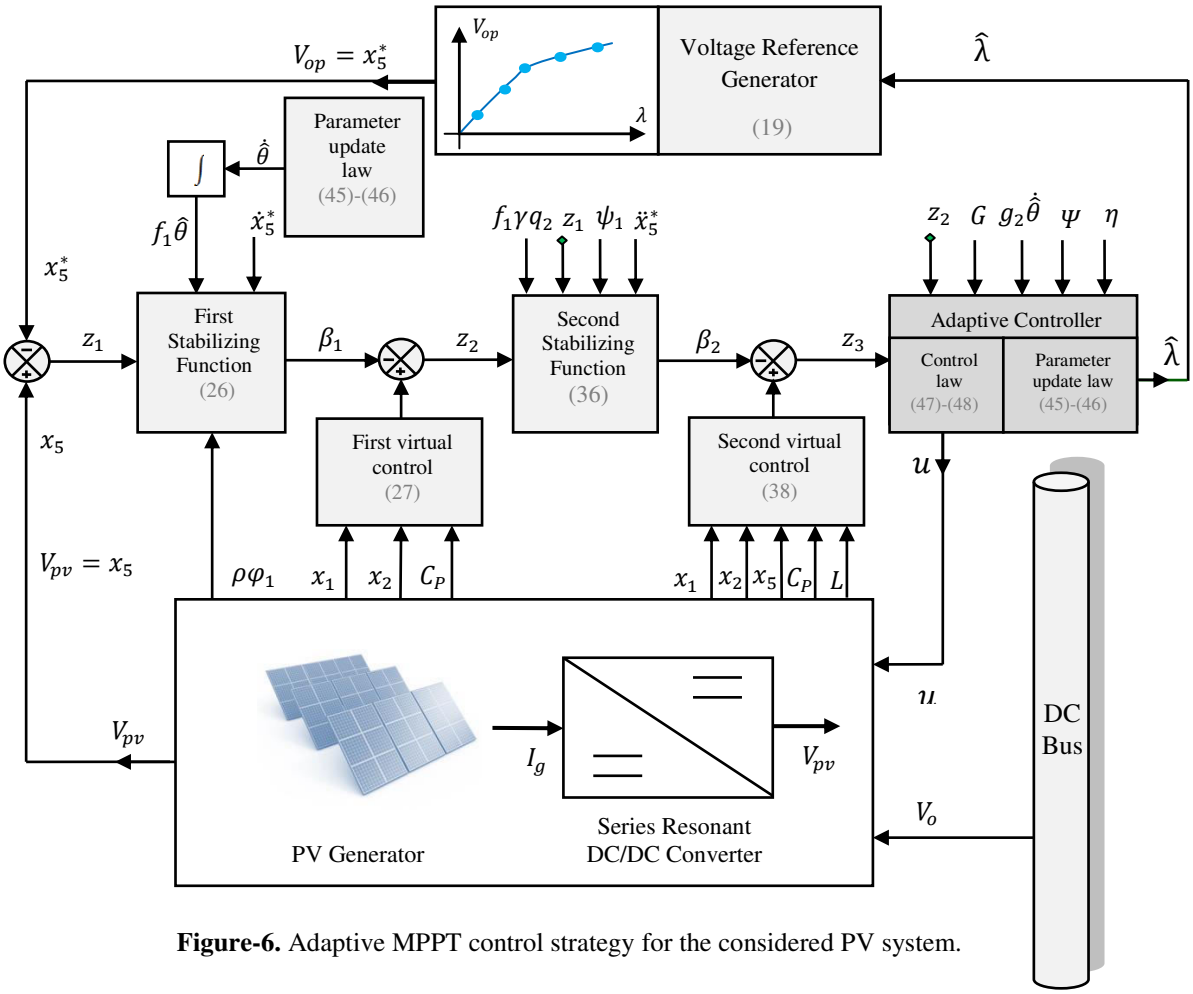

Figure-6. Adaptive MPPT control strategy for the considered PV system.

4. SIMULATION RESULT

4.1 Simulation protocol

The simulation is carried out using MATLAB/SIMULINK software according to the schematic diagram of Figure-6. In simulation, the PV Generator and the SRC are respectively implemented by their physical model Equation (1) and Equations (7-9). The PV generator and resonant converter characteristic are summarized in Table-3.

Table-3. PV System characteristics.

Parameter		Value
PV Generator	n_p	1
	n_s	350
	I_{scr}	3.75 A
	k	$1.38065 * 10^{-23}$ J/K
	q	$1.60220 * 10^{-19}$ C
	K_i	0.00023 A/K
	T_r	298.15 °K
	A	1
	T_c	301.15 °K
Series resonant DC/DC converter	C_P	$16\ x\ 10^{-3}$ F
	L	$0.9\ x\ 10^{-3}$ H
	C	$130\ x\ 10^{-6}$ F
	C_o	$3\ x\ 10^{-3}$ F
	V_o	200 V
	n	5000

In this section, the new Nonlinear Controller (referred by NLC) including the adaptive control law Eqs. (47, 48) and the parameter update law Equations (45, 46) are assessed on their performances. These are first compared with the linear Proportional Integral Controller (referred by PIC). Indeed, a second comparative test of the considered PV system is carried out with a conventional control PV system. The latter consists of a Boost converter controlled by Perturb and Observe (P&O) method. The second comparative test was performed to evaluate the effectiveness of both considered PV system control strategies.

To perform these tests in different operation points, the solar irradiance level (λ) is considered variable over a wide range (step variation: 400 - 900 $\mathrm{W/m^2}$) as shown in Figure-7. The resulting optimal PVG voltage and the corresponding optimal PVG power are respectively described by Figure-8 and Figure-9. These reference signals are constructed using the interpolating polynomial given by Equation (19).

Indeed, in the considered solar irradiance profile (Figure-7), an additive noise was introduced. This latter is a band limited random signal characterized by its mean and variance respectively equal to 1% and 4% of nominal solar irradiance. The initial condition of the SRC state vector was chosen as:

$$\mathrm{X}(0) = [\,-1 \quad -2.02 \quad -0.5 \quad 0.1 \quad 140\,]^{\mathrm{T}}.$$

Note that both resonant and boost converters are implemented by a half-bridge IGBT/Diode model (using Simscape Power Systems blocks). Based on the datasheet characteristics of the IGBT/Diode modules, both switching and conduction losses are evaluated [27].

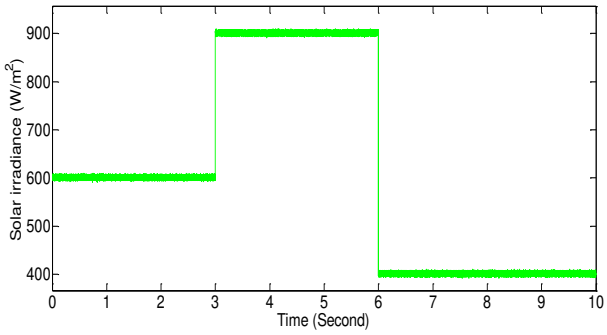

Figure-7. Solar irradiance λ (in $\mathrm{W/m^2}$).

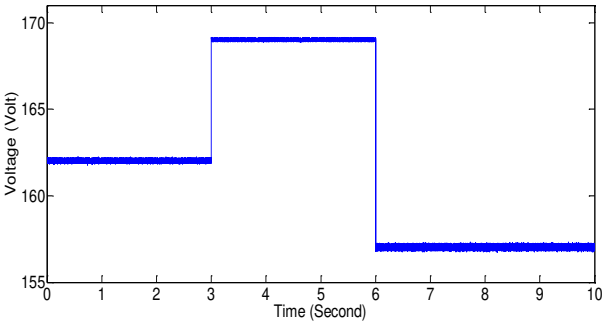

Figure-8. Optimal PVG Voltage $\mathrm{V_{op}}$ (in Volt).

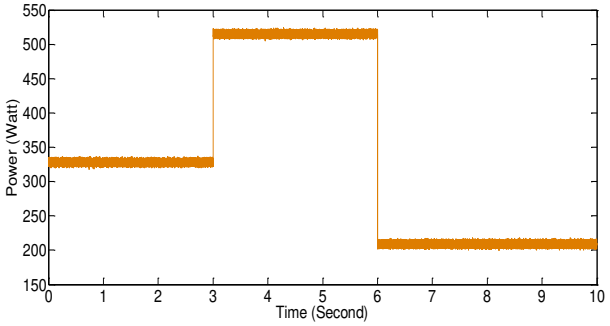

Figure-9. Optimal PVG Power P_{op} (in Watt).

4.2 PI Controller performances

The PIC (defined by $(K_p(1+T_i s)/T_i s)$) is implemented according to the control scheme of Fig.10. The PIC parameters ($K_p = 515$ and $T_i = 9\,ms$) are adjusted based on the time response to different steps. These parameters proved to be convenient when the PVG operates under solar irradiance value around $600\,W/m^2$.

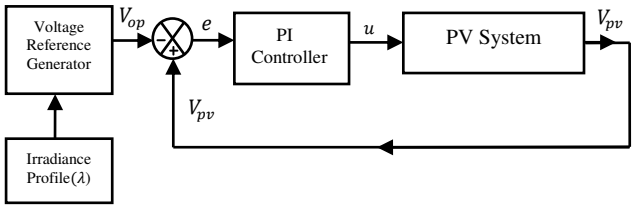

Figure-10. MPP Tracking with PI Controller.

Figure-11 shows that for $t \in [0s\ 3s]$ (where $\lambda \cong 600\,W/m^2$), the PVG voltage perfectly tracks its reference signal. Nevertheless, the tracking performances are no longer maintained for $t \in [3s\ 10s]$. The tracking error signal confirms this performances degradation (see Figure-12). Similarly, Figure-13 shows the corresponding extracted PVG power. Indeed for $t \in [0s\ 3s]$ (where λ is closed to $600\,W/m^2$), the extracted PVG power is optimal and the MPPT objective is achieved. However, this is not the case where λ takes values away from $600\,W/m^2$ (for $t \in [3s\ 10s]$). For instance, Figure-13 shows that during the time interval $[3s\ 6s]$ the extracted PVG power is $481\,W$ while the corresponding optimal value is $514\,W$, (i.e. a power loss in the order of 7%).

This performances degradation is mainly owing to the PV system nonlinear feature. The PIC simulations show that a linear controller cannot ensure the MPPT objective of the PV system equipped with the resonant converter.

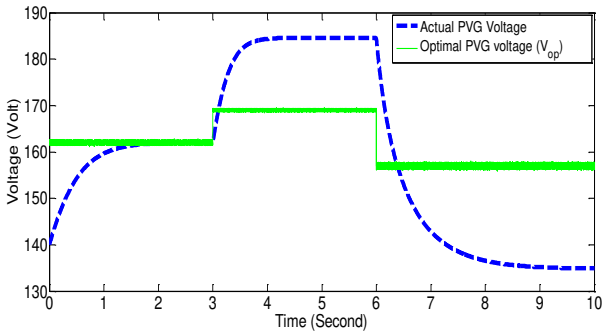

Figure-11. PVG voltage tracking performances with the PI Controller. Solid line: Optimal PVG voltage (in Volt). Dashed line: Actual PVG voltage (in Volt).

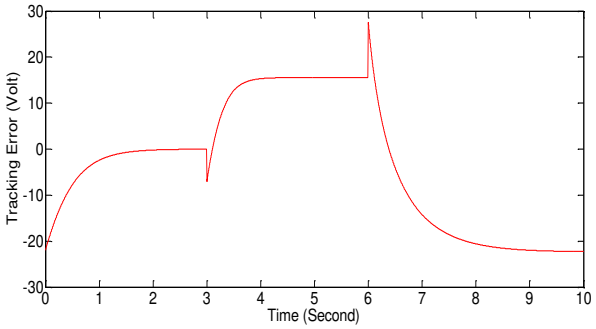

Figure-12. PVG Voltage tracking error with the PI controller (in Volt).

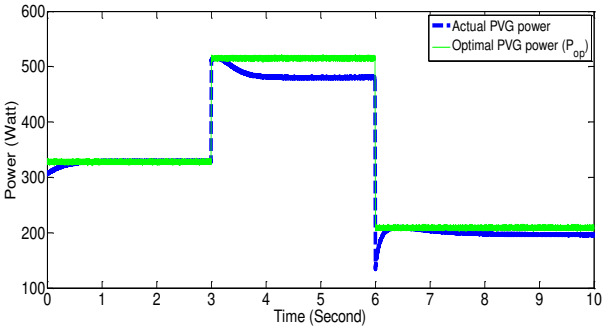

Figure-13. The extracted PVG power with the PI controller. Solid line: Optimal PVG power (in Watt). Dashed line: Actual PVG power (in Watt).

4.3 Nonlinear adaptive Controller performances

This section is devoted to assessing the NLC performances according to the simulated setup of Figure-6. The control law and its update parameter are respectively implemented using Equations (47, 48), Equations (45, 46). The control design parameters are listed in Table-4. These parameters turn out to be suitable for achieving the MPPT objective.

Table-4. NLC parameters.

	Symbol	Value
Adaptive controller	k_1	$7\ x\ 10^2$
	k_2	$9\ x\ 10^2$
	k_3	$14\ x\ 10^2$
Update law	γ	$2\ x\ 10^{-10}$

The controller performances are described by Figures (14-17). Figure-14 shows that whatever the solar irradiance levels, with the NLC, the PVG voltage tracks well its reference signal. Similarly, as shown by Figure-15, the voltage tracking error converges asymptotically to zero in spite of the solar irradiance changes. Note that the transient regime length (of the tracking errors) is adjustable by the choice of the design parameters (k_1, k_2, k_3). Likewise, Figure-16 shows that for all solar irradiance levels, the MPPT objective is achieved. Elsewhere, Figure-17 presents the performances of the solar irradiance adaptation where the estimated parameter reaches its real value. The dynamic of the adaptive error is set by design parameter γ.

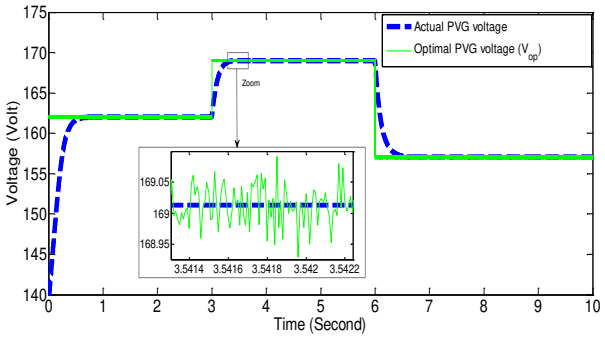

Figure-14. PVG voltage tracking performances with the NLC. Solid line: Optimal PVG voltage (in Volt). Dashed line: Actual PVG Voltage (in Volt).

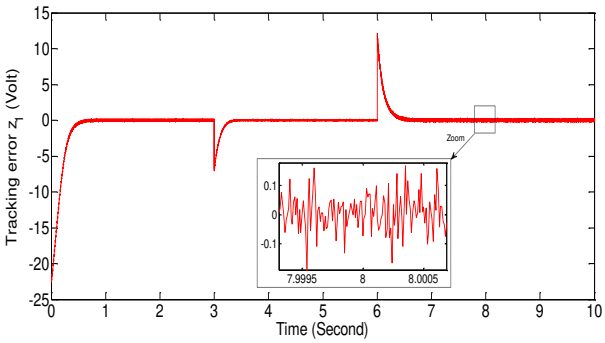

Figure-15. Tracking error z_1 with NLC (in Volt).

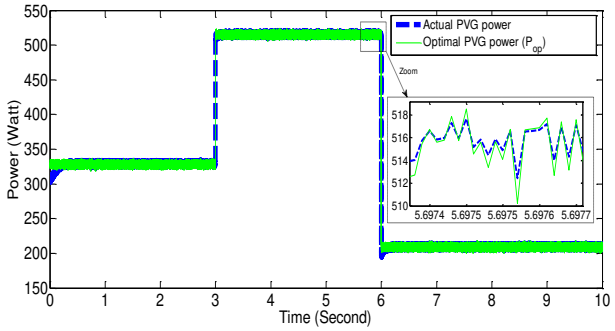

Figure-16. The extracted PVG power with the NLC. Solid line: Optimal PVG power (in Watt). Dashed line: Actual PVG power (in Watt).

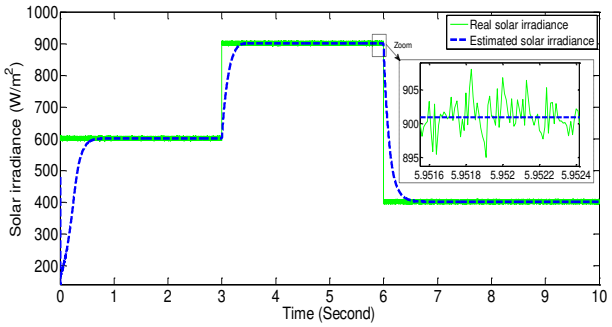

Figure-17. Update law performances. Solid line: The real solar irradiance λ (in W/m^2). Dashed line: The estimated solar irradiance $\hat{\lambda}$ (in W/m^2).

4.4 Conventional control performances

The PV system conventional control is performed according to the simulation setup of Figure-18. The PV system incorporates a Boost converter and a P&O MPPT controller [6, 7]. The conventional control is performed according to the solar irradiance profile depicted in Figure-7.

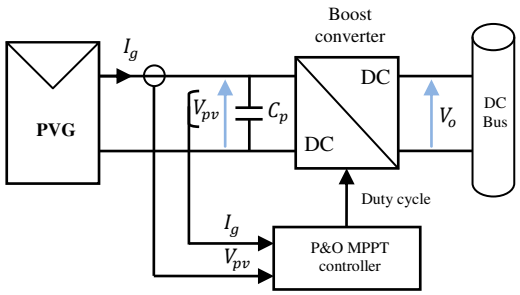

Figure-18. P&O MPPT with boost converter.

The P&O technique is very popular due to simplicity of implementation and easy execution [6, 7]. Recalling that, the P&O control objective is to move the PV operation point towards the corresponding MPP. However, when this latter is located the P&O control oscillates around this power point. This results in oscillations at the PVG voltage (see Figure-19) and consequently at the extracted PVG power (see Figure-20). However, as it's shown in Figure-20 the proposed nonlinear control (NLC) perfectly places the PV operating point at the corresponding MPP.

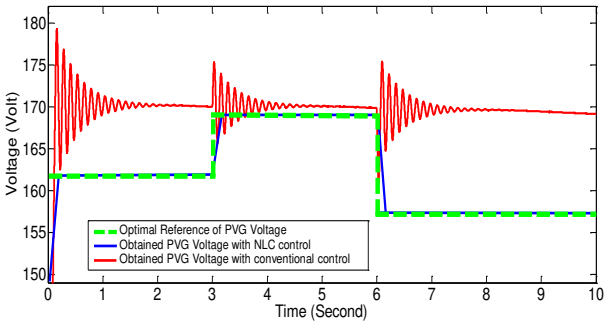

Figure-19. PVG voltage (in Volt). Solid red line: Obtained PVG voltage with the conventional control (using the P&O algorithm and the boost converter). Solid blue line: Obtained PVG voltage with the NLC control (using the resonant converter). Dashed line (green): Optimal reference of the PVG voltage.

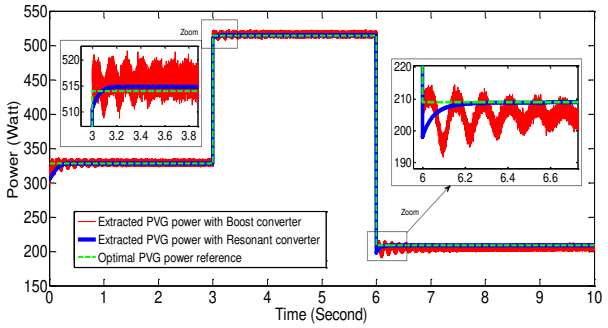

Figure-20. Extracted PVG power (in Watt). Solid red line: Extracted PVG power with the conventional control (using the P&O algorithm and the boost converter). Solid blue line: Extracted PVG power with the NLC control (using the resonant converter). Dashed line (green): Optimal reference of the PVG power.

On the other hand, Figure-21 shows the PVG power recovered at the DC bus, both with the conventional control (P&O algorithm and the boost converter) and the proposed nonlinear control (with the resonant converter). This figure highlights that the recovered DC power with our controller is greater than that obtained with the conventional control strategy (P&O algorithm and the boost converter). Indeed, the power attenuation reached by the boost is due to the converter power losses. In fact, as it is mentioned in this work, the chief advantage of resonant converter is the switching losses optimization.

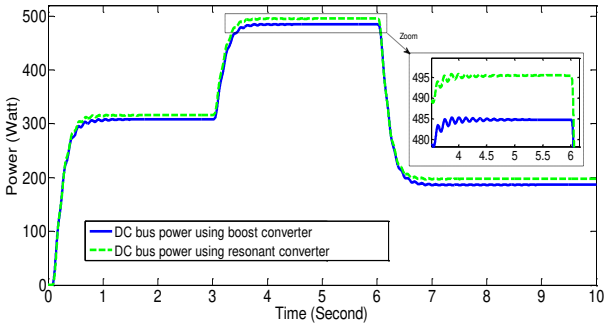

Figure-21. Recovered DC bus power (in Watt). Solid line: with the P&O algorithm and the boost converter. Dashed line: with the NLC control and the resonant converter.

To illustrate the benefits of using the resonant converter, Figure-22 shows the total losses involved in both considered cases. Indeed the boost converter leads to an additional losses during the transfer of PVG power to the DC bus (30 W for $\lambda = 900\ \mathrm{W/m^2}$) compared to the resonant converter (20 W for $\lambda = 900\ \mathrm{W/m^2}$). As a result, the resonant converter optimizes the power transfer from the PV Generator to the DC bus.

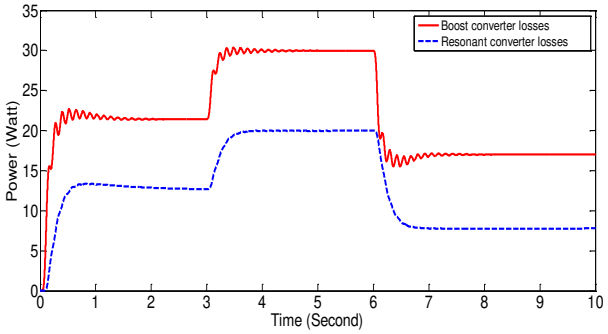

Figure-22. Converter losses (in Watt). Solid line: Boost converter losses. Dashed line: Resonant converter losses.

5. CONCLUSIONS

The present study deals with the MPPT control problem for PV system. For optimizing the switching power losses, the DC/DC converter considered was a series resonant converter. Moreover, a cheap solution, not based on solar irradiance sensor, was developed. Indeed, based on the PV system model Eqs. (14-18), an adaptive nonlinear controller (NLC) is developed using the Backstepping approach. The developed controller involves the adaptive update law Eqs. (45, 46) and the control law Eqs. (47, 48). For achieving the MPPT objective, the closed loop PV system stability was formally demonstrated (Theorem) resulting in a global and asymptotic stability. Numerical simulations were performed to highlight the tracking performances of the proposed controller compared to the linear PI Controller and the P&O controller. The comparison with the conventional control has shown that the proposed nonlinear control is quite able to achieve the MPPT objective. Thanks to the resonant converter, the energy transfer to the DC bus was optimized with low power losses.

REFERENCES

[1] 2014. International Energy Agency statistics: CO2 emissions from fuel combustion. www.iea.org.

[2] Gonzatti F., Kuhn V.N., Miotto M., Ferrigolo F.Z., Farret F.A. 2016. Distinct Renewable Energy Systems Maximized by P&O Algorithm. Journal of Control, Automation and Electrical. Systems. 27, 310-316.

[3] Xiao W., Dunford W.G., Palmer P.R, Capel A. 2007. Regulation of Photovoltaic Voltage. IEEE Trans. Ind. Electron. 54, 1365–1374.

[4] Villalva M.G., de Siqueira T.G., Ruppert E. 2010. Voltage regulation of photovoltaic arrays: small-signal analysis and control design. Power Electro. 3, 869-880.

[5] Ghassami A.A., Sadeghzadeh S.M., Soleimani A. 2013. A high performance maximum power point tracker for PV systems. Electrical Power and Energy Syst. 53, 237-243.

[6] Esram T., Chapman P.L. 2007. Comparison of Photovoltaic Array Maximum Power Point Tracking Techniques. IEEE Trans. Enr. Conver. 22, 439-449.

[7] Kamarzaman, N.A., Tan, C.W. 2014. A comprehensive review of maximum power point tracking algorithms for photovoltaic systems. Renew. Sust. Enr. Rev. 37, 585–598.

[8] Bendib B., Krim F., Belmili H., Almi M.F., Boulouma S. 2014. Advanced Fuzzy MPPT Controller for a Stand-alone PV System. Ener. Proc. 50, 383-392.

[9] Rai, A.K., Kaushika, N.D., Singh, B., Agarwal, N. 2011. Simulation model of ANN based maximum power point tracking controller for solar PV system. Sol. Enr. Mat. Sol. Cells. 95, 773-778.

[10] Pradhan R., Subudhi B. 2015. Design and real-time implementation of a new auto-tuned adaptive MPPT control for a photovoltaic system. Elec Power Enr. Syst. 64,792-803.

[11] Massaoudi, Y., Damak, T., Ghamgui, M., Mehdi, D. 2013. Comparison between a Backstepping Mode Control and a Sliding Mode Control for a Boost DC-DC Converter of a Photovoltaic Panel. 10th

International Multi-Conference on Systems, Signals & Devices. 1-7.

[12] Chu C.C., Chen, C.L. 2009. Robust maximum power point tracking method for photovoltaic cells: A sliding mode control approach. Sol. Enr. 83, 1370-1378.

[13] El Fadil, H., Giri, F. 2011. Climatic sensorless maximum power point tracking in PV generation systems. Control Eng. Pract. 19, 513-521.

[14] Sanders S.R., Noworolski J.M., Liu X.Z., Verghese G. 1991. Generalized averaging method for power conversion circuits. IEEE Trans. Power Electro. 6, 251–259 (1991)

[15] Krstic M., Kanellakopoulos, I., Kokotovic P. 1995. Nonlinear and adaptive control design. John Wiley and Sons.

[16] Cui R., Guo J., Mao Z. 2015. Adaptive backstepping control of wheeled inverted pendulums models. Nonlinear Dyn. 79, 501-511.

[17] Sun L., Zheng Z. 2015. Nonlinear adaptive trajectory tracking control for a stratospheric airship with parametric uncertainty. Nonlinear Dyn. 82, 1419-1430.

[18] Bayod-Rujula A.A., Cebollero-Abian J.A. 2014. A novel MPPT method for PV systems with irradiance measurement. Sol. Enr. 109, 95-104.

[19] Moçambique N.E.M., Ottoboni K.A., Fuzato G.H.F., *et al*. 2015. Tracking Algorithms and Voltage Controllers Used to Obtain the Maximum Power Point of PV Arrays. J. Control. Autom. Electric. Syst. 26, 661-674.

[20] Qi C., Ming Z. 2012. Photovoltaic Module Simulink Model for a Stand-alone PV System. Phys. Procedia. 24, 94-100.

[21] Ferrieux J.P., Forest F. 1999. Alimentations à découpage - Convertisseurs à résonance, DUNOD, 3ème édition revue et augmentée.

[22] Giri F., El Maguiri O., El Fadil H., Chaoui F. Z. 2011. Nonlinear adaptive output feedback control of series resonant DC-DC converters. Control Eng. Practice. 19, 1238-1251.

[23] Amghar B., Darcherif A.M., Barbot J.P. Boukhetala D. 2014. Modeling and control of series resonant converter for high voltage applications. IEEE Int. Conf. ENERGYCON. 216–221.

[24] Stankovic A.M., Perreault D.J., Sato K. 1999. Synthesis of dissipative nonlinear controllers for series resonant DC/DC converters. IEEE Trans. Power Electro. 14, 673-682.

[25] Carrasco J.M., Galvan E., Valderrama G.E., Ortega R., Stankovic A.M. 2000. Analysis and Experimentation of Nonlinear Adaptive Controllers for the Series Resonant Converter. IEEE Trans. Power Electro. 15, 536-544.

[26] Naik S.M., Kumar P.R., Ydstie B.E. 1992. Robust Continuous-Time Adaptive Control by Parameter Projection. IEEE Trans. autom. Control. 37, 182-197.

[27] Giroux P., Sybille G., Tremblay O. 2012. Loss Calculation and Thermal Model in a Buck Converter. Hydro-Quebec Research Institute.

Appendix A. Proof of Theorem

Part 1 Substituting Eq.(47) in Eq.(44), one has:

$$\dot{V}_3 = -k_1 {z_1}^2 - k_2 {z_2}^2 - k_3 {z_3}^2 - z_2 f_1 \left(\gamma q_2 - \dot{\hat{\theta}}\right) + \tilde{\theta}\left(-\frac{\dot{\hat{\theta}}}{\gamma} + q_3\right) + \eta z_3 \quad \text{(B1)}$$

With Equation (46), two cases can be distinguished:

- First case where $\hat{\theta}^2 \leq D^2$, Equation (B1) becomes:

$$\dot{V}_3 = -k_1 {z_1}^2 - k_2 {z_2}^2 - k_3 {z_3}^2 + z_3(\eta + \gamma f_1 f_3 z_2) \quad \text{(B2)}$$

This clearly suggests the choice of parameter η defined in Equation (48). This choice makes possible to simplify (B2), which reduces to:

$$\dot{V}_3 = -k_1 {z_1}^2 - k_2 {z_2}^2 - k_3 {z_3}^2 \quad \text{(B3)}$$

- Second case where $\hat{\theta}^2 > D^2$, by using Equations (35,25) equation (B1) becomes:

$$\dot{V}_3 = -k_1 {z_1}^2 - k_2 {z_2}^2 - k_3 {z_3}^2 - z_2 \gamma f_1 (z_1 f_1 + z_2 f_2) \quad \text{(B4)}$$

with Equations (31,24), Equation (B4) becomes:

$$\dot{V}_3 = -k_1 {z_1}^2 - k_2 {z_2}^2 - k_3 {z_3}^2 - \gamma f_1^2 z_1 z_2 - \gamma k_1 f_1^2 z_2^2 + \gamma f_1^2 z_2^2 \rho A_g exp\left(A_g x_5\right) \quad \text{(B5)}$$

Furthermore, in practice the PV voltage x_5 is bounded. Indeed, x_5 verifies: $0 \leq x_5 \leq V_M$, where $V_M = n_s\, 0{,}6$. Then, time derivative of the Lyapunov's candidate function given by Eq.(B5) checks the following inequality:

$$\dot{V}_3 \leq -\left(k_1 - \frac{\gamma {f_1}^2}{2}\right){z_1}^2 - \left(k_2 - \gamma {f_1}^2(\varrho + 0.5)\right)\mathrm{z}_2^2 - k_3 {z_3}^2 \quad \text{(B6)}$$

with $\varrho = \rho A_g exp(A_g V_M)$. Let chooses the design parameter $k_1, k_2,$ and k_3 such as:

$$k_1 > \frac{\gamma {f_1}^2}{2}, \quad k_2 > \gamma {f_1}^2(\varrho + 0.5) \text{ and } k_3 > 0 \quad \text{(B7)}$$

With respect to Eq. (B7), Eqs. (B6, B3) shows that in all mentioned cases $\dot{V}_3$ is negative semi-definite. Then using the Barbalat's lemma, the error vector $Z = [z_1, z_2, z_3]^T$ vanishes asymptotically.

Part 2 Recall that the error vector dynamic is given by:

$$\dot{Z} = \bar{M}Z + F\tilde{\theta} \quad \text{(B8)}$$

knowing that in the steady state the vector Z vanishes asymptotically, Eq.(B8) shows that (in the steady state) the estimation error $\tilde{\theta}$ converges also to 0.

Appendix B. The used notations in the control design

Expressions of used notations in the control design	
Parameter	**Expression**
$G(x_1, x_2, x_5)$	$-\frac{8}{\pi^2 L C_p}\frac{1}{\sqrt{{x_1}^2 + {x_2}^2}}\, x_1 x_5$
$f_3(x_1, x_2, x_5)$	$\frac{8}{\pi^2 L {C_p}^2}\frac{x_2}{\sqrt{{x_1}^2 + {x_2}^2}} + \frac{\rho\, A_g}{C_p}\, exp(A_g x_5)\left(-\frac{A_g}{C_p}\left(\hat{\theta} + z_2\,\frac{\gamma}{C_p}\right) + 2\, A_g\, \rho\, exp(A_g x_5) - A_g\, \rho + A_g\,\frac{4}{\pi C_p}\sqrt{{x_1}^2 + {x_2}^2}\right) + \frac{\gamma}{{C_p}^3}\left(1 + \left(k_1 - \rho A_g exp(A_g x_5)\right)^2\right) - \frac{({k_1}^2 - 1)}{C_p} + \frac{(k_1 + k_2)}{C_p}\left(k_1 - \rho A_g exp(A_g x_5)\right)$
$g_2(x_5)$	$-\frac{(k_1 + k_2)}{C_p} + \frac{\rho\, A_g}{C_p}\, exp(A_g x_5)\left(1 + \frac{\gamma}{{C_p}^2}\right) - \frac{\gamma}{{C_p}^3} k_1$
$\Psi(X)$	$\frac{8}{\pi^2 L C_p}\frac{1}{\sqrt{{x_1}^2 + {x_2}^2}}\left(-\frac{1}{L}x_4 x_5 + \frac{2}{n\pi L}\frac{V_0 x_1 x_5}{\sqrt{{x_1}^2 + {x_2}^2}} - \frac{2{x_5}^2}{\pi L} + \frac{x_2\hat{\theta}}{C_p} - \rho\varphi_1 x_2 - \frac{4x_2}{\pi C_p}\sqrt{{x_1}^2 + {x_2}^2}\right) - \frac{8}{\pi^2 L C_p}\frac{x_2 x_5}{({x_1}^2 + {x_2}^2)}\left(-\frac{(x_1 x_3 + x_2 x_4)}{L\sqrt{{x_1}^2 + {x_2}^2}} - \frac{2x_2 x_5}{\pi L\sqrt{{x_1}^2 + {x_2}^2}}\right) - A_g\rho\, exp(A_g x_5)\left(\frac{\hat{\theta}}{C_p} - \rho\varphi_1 - \frac{4}{\pi C_p}\sqrt{{x_1}^2 + {x_2}^2}\right)\left[-2\, A_g\rho\, exp(A_g x_5) + A_g\rho - A_g\frac{4}{\pi C_p}\sqrt{{x_1}^2 + {x_2}^2}\right] + \frac{4}{\pi C_p}A_g\rho\, exp(A_g x_5)\left(-\frac{(x_1 x_3 + x_2 x_4)}{L\sqrt{{x_1}^2 + {x_2}^2}} - \frac{2x_2 x_5}{\pi L\sqrt{{x_1}^2 + {x_2}^2}}\right) + \frac{4}{\pi L C_p}\cdot\left[\frac{1}{\sqrt{{x_1}^2 + {x_2}^2}}\cdot\left(-\frac{({x_3}^2 + {x_4}^2)}{L} - \frac{2V_0(x_2 x_3 - x_1 x_4)}{n\pi L\sqrt{{x_1}^2 + {x_2}^2}} - \frac{2x_4 x_5}{\pi L} + \frac{({x_1}^2 + {x_2}^2)}{C}\right) - \frac{(x_1 x_3 + x_2 x_4)}{({x_1}^2 + {x_2}^2)}\left(-\frac{(x_1 x_3 + x_2 x_4)}{L\sqrt{{x_1}^2 + {x_2}^2}} - \frac{2x_2 x_5}{\pi L\sqrt{{x_1}^2 + {x_2}^2}}\right)\right] - (-k_1 z_1 + z_2)({k_1}^2 - 1) + \left(-z_1 - k_2 z_2 + z_3 - \frac{\gamma}{C_p}q_2\right)(k_1 + k_2) - \frac{\rho\, A_g}{C_p}\, exp(A_g x_5)\left(\frac{\hat{\theta}}{C_p} - \rho\varphi_1 - \frac{4}{\pi C_p}\sqrt{{x_1}^2 + {x_2}^2}\right)\left(A_g\,\hat{\theta} + z_2\, A_g\,\frac{\gamma}{C_p}\right) + \frac{\gamma}{{C_p}^2}(-k_1 z_1 + z_2) + \frac{\gamma}{{C_p}^2}\left(k_1 - \rho A_g exp(A_g x_5)\right)\left(-z_1 - k_2 z_2 + z_3 - \frac{\gamma}{{C_p}^2}z_1 - \frac{\gamma}{{C_p}^2}z_2\left(k_1 - \rho A_g exp(A_g x_5)\right)\right) - \dddot{x}_5^*$